RSC Advances

PAPER

View Article Online
View Journal | View Issue

Check for updates

Cite this: *RSC Adv.*, 2018, **8**, 26309

Evaluation of thin film fuel cells with Zr-rich $BaZr_xCe_{0.8-x}Y_{0.2}O_{3-\delta}$ electrolytes ($x \geq 0.4$) fabricated by a single-step reactive sintering method

Seongwoo Jeong,[a] Taisei Kobayashi,[a] Kosuke Kuroda,[a] Hyuna Kwon,[b] Chunyu Zhu,[c] Hiroki Habazaki[c] and Yoshitaka Aoki *[c]

This paper reports a survey of power generation characteristics of anode-supported thin film fuel cells with Zr-rich $BaZr_xCe_{0.8-x}Y_{0.2}O_{3-\delta}$ (x = 0.4, 0.6, 0.7, and 0.8) proton-conducting electrolytes, which were fabricated by single step co-firing with $Zn(NO_3)_2$ additives at a relatively low temperature (1400 °C). The grain sizes significantly increased to several μm for x = 0.4 and 0.6, whereas the grain sizes remained in the sub-μm ranges for x = 0.7 and 0.8, which resulted in large gaps of the fuel cell performances at x over and below 0.6. The cells for x = 0.4 and 0.6 exhibited efficient power generation, yielding peak powers of 279 and 336 mW cm^{-2} at 600 °C, respectively, which were higher than those of the corresponding cells previously reported. However, the performances abruptly deteriorated with the increasing x to more than 0.7 because the electrolyte films were highly resistive due to the coarse-grained microstructures. Impedance spectroscopy for the dense sintered $BaZr_xCe_{0.8-x}Y_{0.2}O_{3-\delta}$ discs confirmed that the total proton conductivity of $BaZr_{0.6}Ce_{0.2}Y_{0.2}O_{3-\delta}$ was higher than that of $BaZr_{0.4}Ce_{0.4}Y_{0.2}O_{3-\delta}$ at temperatures above 500 °C despite relatively small grain sizes. In addition, $BaZr_{0.6}Ce_{0.2}Y_{0.2}O_{3-\delta}$ cells could gain a stable current throughout a continuous run for a few days under CO_2-containing fuel supply, which was due to high fraction of thermodynamically stable $BaZrO_3$ matrices. It was demonstrated that $BaZr_{0.6}Ce_{0.2}Y_{0.2}O_{3-\delta}$ is a promising electrolyte for proton-conducting ceramic fuel cells with excellent proton conductivity and CO_2 tolerance at intermediate temperatures.

Received 2nd June 2018
Accepted 9th July 2018

DOI: 10.1039/c8ra04724c

rsc.li/rsc-advances

Open Access Article. Published on 23 July 2018. Downloaded on 12/15/2025 1:50:24 AM.
This article is licensed under a Creative Commons Attribution-NonCommercial 3.0 Unported Licence.

1. Introduction

Solid oxide fuel cells (SOFCs) have attracted much attention because of their fuel flexibility, high efficiency, and lack of requirement of expensive noble metal catalysts;[1–3] however, their high operating temperature causes high fabrication and operation cost and durability issues,[4] which consequently limit their application and commercialization. Hence, lowering the operating temperature to intermediate temperatures (IT), *i.e.*, 400–700 °C is important for further applications.

High temperature proton conductors can decrease the operating temperature, because they have lower activation energy (0.3–0.6 eV) for ionic conduction than typical oxide-ion conductors such as $Zr_{1.8}Y_{0.2}O_3$ (0.8 eV).[5] Materials including $BaCe_{0.9}Y_{0.1}O_3$ and $BaZr_{0.8}Y_{0.2}O_3$ possess higher conductivities than $Zr_{1.8}Y_{0.2}O_3$ at temperatures below 700 °C.[6] Therefore, protonic ceramic fuel cells (PCFCs) are promising for operations at IT. Although $BaCeO_3$-based oxides display excellent proton conductivity,[7] they are thermodynamically unstable in a CO_2-containing atmosphere below 800 °C, resulting in their decomposition to $BaCO_3$ and CeO_2.[8] In contrast, $BaZrO_3$ is thermodynamically stable in a CO_2-rich atmosphere; thus, the partial replacement of Ce with Zr can improve the stability in a CO_2-rich atmosphere.[9,10] Solid solutions, *i.e.*, $BaCe_{1-x-y}Zr_xM_yO_3$ (M = Y, Gd, *etc.*) tend to be more tolerant to CO_2 with the increasing Zr contents[9,10] and thus, Zr-rich $BaCe_{1-x-y}Zr_xM_yO_3$ is desirable as a practical electrolyte for IT-PCFCs. Meanwhile, the fuel cell performances are still limited because the solid solutions tend to show poor sinterability with increasing Zr contents due to high refractory nature of $BaZrO_3$ moieties, and their coarse-grained microstructures have large grain-boundary resistances of electrolytes.[9,10] Normally, Zr-rich phases require sintering temperatures over 1600 °C (ref. 11) for sufficient grain growth, but such high temperature sintering causes BaO evaporation and undesired reaction at the interface between the electrolyte and cermet anodes, which significantly increases electrolyte resistances of fuel cells.[12,13] Hence, it is necessary to fabricate highly efficient anode-supported cells with large-

[a]*Graduate School of Chemical Sciences and Engineering, Hokkaido University, N13W8 Kita-ku, Sapporo, 060-8628 Japan*

[b]*Department of Energy Resources Engineering, College of Engineering, Seoul National University, 1 Gwanak-ro, Gwanak-gu, Seoul 08826, Korea*

[c]*Faculty of Engineering, Hokkaido University, N13W8 Kita-ku, Sapporo, 060-8626 Japan. E-mail: y-aoki@eng.hokudai.ac.jp; Tel: +81-11-706-6752*

Open Access Article. Published on 23 July 2018. Downloaded on 12/15/2025 1:50:24 AM.
This article is licensed under a Creative Commons Attribution-NonCommercial 3.0 Unported Licence.

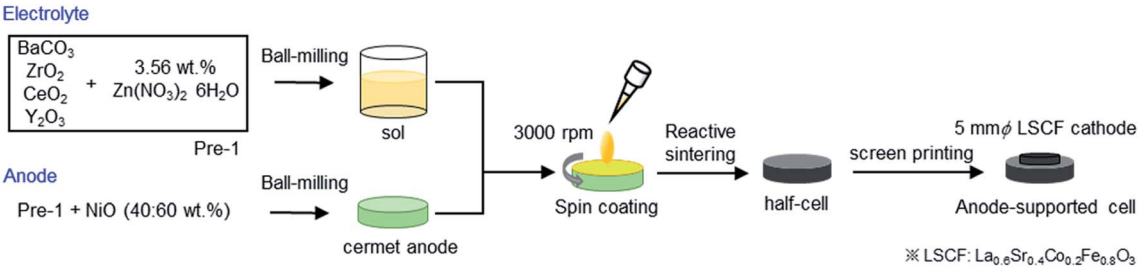

Fig. 1 The schematic diagram for SSRS fabrication of anode-supported cells.

grained electrolyte films using high Zr-content $BaCe_{1-x-y}Zr_xM_yO_3$ ($1 - x - y < x$) under moderate sintering conditions.

In many scientific studies, wet chemical processes, such as co-precipitation and combustion methods, were employed to prepare fine green powders of $BaZr_xCe_{0.8-x}Y_{0.2}O_3$, whereas such powders did not lead to highly dense ceramics with more than 90% relative density by sintering at temperatures below 1500 °C, especially for $x > 0.4$.[14] Recently, Duan *et al.* developed a significantly simplified and cost-effective solid-state reactive sintering (SSRS) method to fabricate anode-supported thin film electrolyte PCFC with $BaZr_{0.1}Ce_{0.7}Y_{0.1}Yb_{0.1}O_3$ (BZCYYb).[15] In the SSRS process, phase formation, densification, and grain growth were conducted at a single high-temperature sintering step, and the resultant electrolyte films were significantly densified despite lower (200–400 °C) sintering temperatures compared to the observations of the conventional process.[16] The resultant cells could conduct efficient power generation even at 500 °C.[15] In this study, we successfully fabricated anode-support thin film fuel cells based on high Zr-content $BaZr_xCe_{0.8-x}Y_{0.2}O_3$ ($x = 0.4$, 0.6, 0.7, and 0.8) electrolytes (~30 μm thickness) by modifying the SSRS method with a single sintering step at around 1400 °C. $BaZr_{0.6}Ce_{0.2}Y_{0.2}O_3$-based cells achieved the highest power output among the four studied cells, which was due to the superior proton conductivity at elevated temperatures; they were also highly tolerant to CO_2 due to the relatively high fraction of the thermodynamically stable zirconates, which demonstrated that $BaZr_{0.6}Ce_{0.2}Y_{0.2}O_3$ is a promising electrolyte of intermediate temperature PCFC.

2. Experimental details

2.1 Fabrication of thin film fuel cells with porous anode supports

The anode-supported cells were fabricated by solid-state reactive sintering (SSRS) of green pellets with alternative $Zn(NO_3)_2$ sintering aids instead of commonly used NiO aids.[15,18,19] The fabrication process is schematically represented in Fig. 1. Precursor powders of $BaZr_xCe_{0.8-x}Y_{0.2}O_{3-\delta}$ ($x = 0.4$, 0.6, 0.7, and 0.8) were prepared by mixing stoichiometric amounts of starting materials: $BaCO_3$ (High Purity Chemicals, 99.95%), CeO_2 (High Purity Chemicals, 99.99%), ZrO_2 (High Purity Chemicals, 98%), and Y_2O_3 (High Purity Chemicals, 99.99%) with addition of 3.56 wt% of $Zn(NO_3)_2 \cdot 6H_2O$ (Wako chemicals, 99.9%) as a sintering aid. The mixtures were ball-milled in ethanol for 24 h and subsequently dried at 80 °C; thus, precursor powders of $BaZr_xCe_{0.8-x}Y_{0.2}O_{3-\delta}$ (denoted as Pre-1 hereafter) were obtained. For Ni/$BaZr_xCe_{0.8-x}Y_{0.2}O_{3-\delta}$ anode supports, Pre-1 and NiO were blended at a weight ratio of 40 : 60 in ethanol and ball-milled for 48 h. The obtained mixed powders were uniaxially pressed into green pellets (12 mm ϕ, 1.2 mm d) under 20 MPa and subsequently pressed under a hydrostatic pressure of 100 MPa in an isostatic press. The precursor layers of electrolyte films were spin-coated on the green pellets by using a MISAKA 1H-D7 spin-coater. The sols were prepared by dispersing Pre-1 in a solution containing dispersant (20 wt% polyethyleneimine (M_w 28 000) dissolved in α-terpineol) and binder (5 wt% surfactant dissolved in α-terpineol) at a weight ratio of 10 : 3 : 1, and they were spin-coated on the surfaces of the green pellets at 3000 rpm for 40 s. After spin coating, the pellets were dried at room temperature and co-fired at 1400 °C for 8 h, 12 h, 12 h, and 18 h for $x = 0.4$, 0.6, 0.7, and 0.8, respectively, in air. The pellets were highly densified by sintering, which resulted in a compact ceramic disc with *ca.* 9 mm ϕ × 1 mm d.

The back sections of the sintered discs were polished with 1000 SiC abrasive sandpapers and then, Pt paste was applied as a current collector attached with a gold wire (0.1 mm ϕ). Finally, $La_{0.6}Sr_{0.4}Co_{0.2}Fe_{0.8}O_{3-\delta}$ (LSCF) button electrode (5 mm ϕ) was deposited on the other side as a porous cathode by screen-printing with a commercial LSCF paste (Fuelcellmaterials)

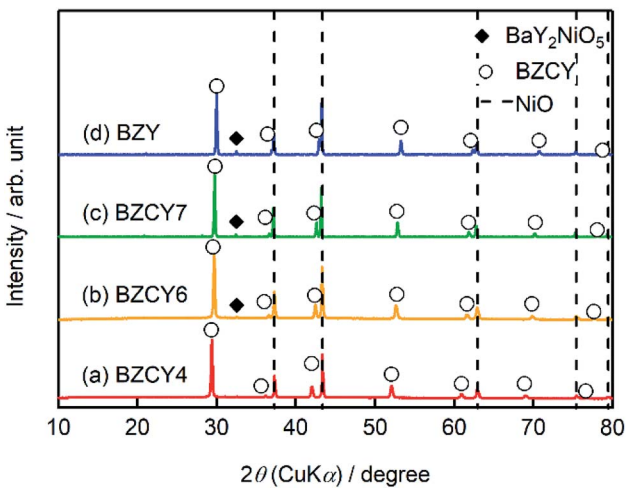

Fig. 2 XRD patterns of the thin film fuel cells based on (a) BZCY4, (b) BZCY6 (c) BZCY7, and (d) BZY electrolytes prepared by the SSRS process shown in Fig. 1. For the measurements, the sintered sample is pulverized without screen-printing LSCF.

This journal is © The Royal Society of Chemistry 2018

Open Access Article. Published on 23 July 2018. Downloaded on 12/15/2025 1:50:24 AM.
This article is licensed under a Creative Commons Attribution-NonCommercial 3.0 Unported Licence.

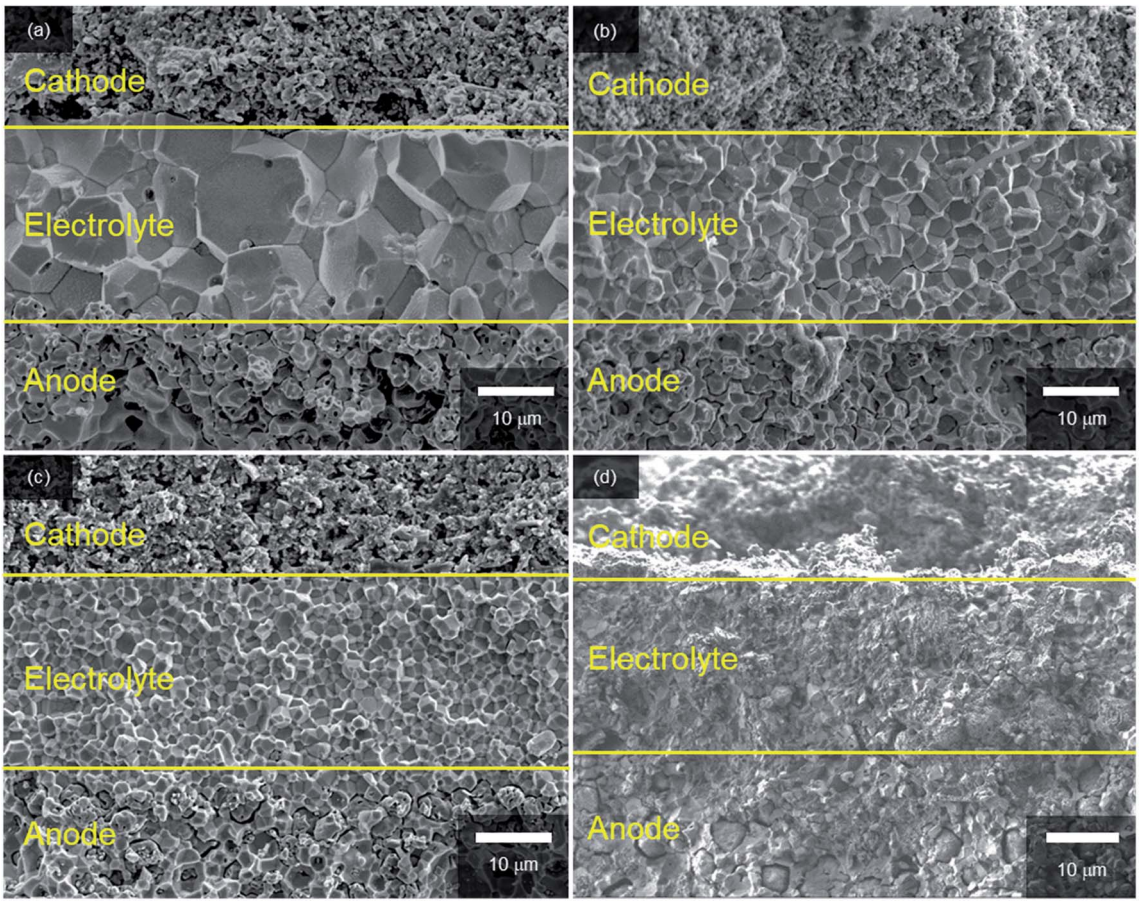

Fig. 3 Cross-section SEM micrographs of anode-supported cells with (a) BZCY4, (b) BZCY6, (c) BZCY7 and (d) BZY electrolytes.

and post-annealing at 700 °C. A Pt mesh was used as a current collector of the cathode.

Bulk ceramics for conductivity measurements of $BaZr_x$-$Ce_{0.8-x}Y_{0.2}O_{3-\delta}$ ($x = 0.4$ and 0.6) were prepared by a process similar to the SSRS process. Pre-1 powders were uniaxially pressed into green pellets (12 mm ϕ, 1.2 mm d) under 20 MPa and subsequently pressed under a hydrostatic pressure of 100 MPa in an isostatic press. The pellets, thus prepared, were reactive-sintered at 1400 °C for 8 or 12 h in air. Both faces of the sintered discs were polished by an SIC paper and then, Pt paste was applied as a current collector.

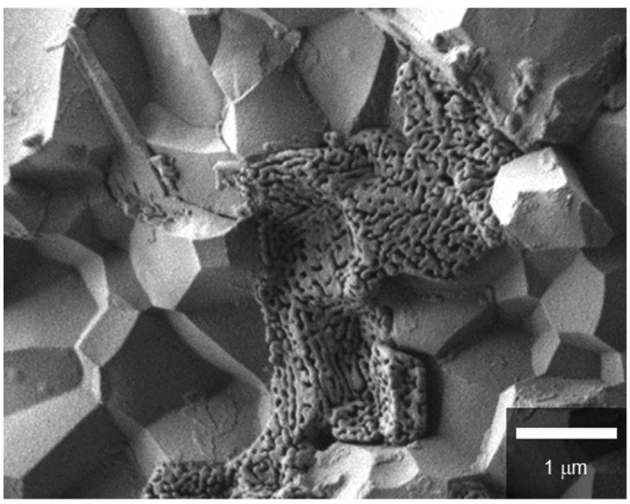

Fig. 4 High magnification image of BZY electrolyte thin film.

The phase purity was checked by X-ray diffraction (XRD) analysis in the 2θ range between 10° and 80° at a scan rate of 5° min^{-1} using Rigaku Ultima IV (CuKα radiation). For the XRD measurements, the cells before screen-printing LSCF layers were pulverized in a mortar. The microstructures of the fabricated cells were examined using a field emission scanning electron microscope (FESEM; SIGMA500, ZEISS). The composition of the electrolytes was evaluated by energy-dispersive X-ray analysis (EDX; JEOL-S100).

2.2 Electrochemical performance of a single cell

A single cell thus prepared was mounted in a lab-constructed fuel cell test station. The cathode compartment was sealed by a molten glass ring gasket. Before fuel cell tests, the cathode side was exposed to humidified Ar gases, and the anode side was exposed to humidified 10%-H_2/Ar mix gases at 700 °C for 1 h to covert NiO to metallic Ni; thus, a porous Ni/$BaZr_x$-$Ce_{0.8-x}Y_{0.2}O_{3-\delta}$ cermet anode was prepared. All humidified gases were prepared by bubbling in Milli-Q deionized water at

Open Access Article. Published on 23 July 2018. Downloaded on 12/15/2025 1:50:24 AM.
This article is licensed under a Creative Commons Attribution-NonCommercial 3.0 Unported Licence.

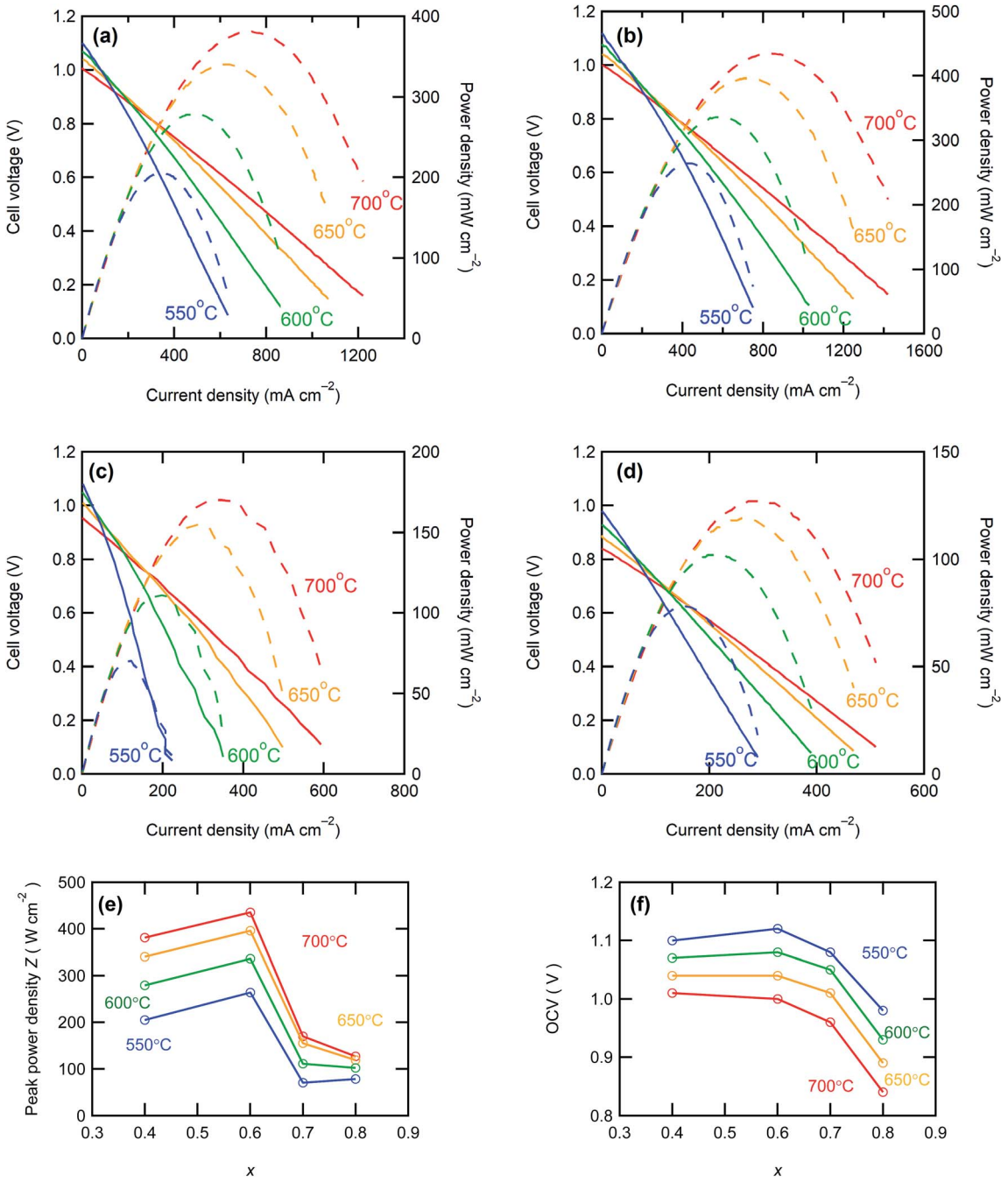

Fig. 5 *I–V* and *I–P* curves of fabricated anode-supported cells consisting of (a) BZCY4, (b) BZCY6, (c) BZCY7 and (d) BZY. Solid lines show *I–V* characteristics and dashed lines show *I–P* characteristics. Summary of (e) peak power densities and (f) open circuit voltages.

room temperature at a flow rate of 50 sccm, such that the corresponding water partial pressure (p_{H_2O}) equalled 3 kPa. For fuel cell tests, humidified hydrogen was fed to anode, and humidified air was supplied to the cathode side at a rate of 50 sccm. The electrochemical performances of the cells were evaluated in the temperature range of 550–700 °C. Impedance spectroscopy was conducted with a Solartron 1260A frequency response analyzer implemented with a Solartron 1287 potentiostat in the frequency range of 10^6 to 0.1 Hz with ac amplitude of 30 mV under OCV condition. Current–voltage (*I–V*) and current–power (*I–P*) characteristics were recorded on the same apparatus. CO_2 durability tests were performed by monitoring the current outputs under potentiostatic conditions while feeding 1%-CO_2/H_2 mixed gases to the anode for 2 days.

3. Results & discussion

3.1 Material characterization

Hereafter, $BaZr_xCe_{0.8-x}Y_{0.2}O_{3-\delta}$ with $x = 0.4$, 0.6, 0.7, and 0.8 are denoted as BZCY4, BZCY6, BZCY7, and BZY, respectively. Fig. 2 represents the powder X-ray diffraction (XRD) patterns of the pulverized thin film fuel cells without screen-printing LSCF

 This journal is © The Royal Society of Chemistry 2018

Open Access Article. Published on 23 July 2018. Downloaded on 12/15/2025 1:50:24 AM.
This article is licensed under a Creative Commons Attribution-NonCommercial 3.0 Unported Licence.

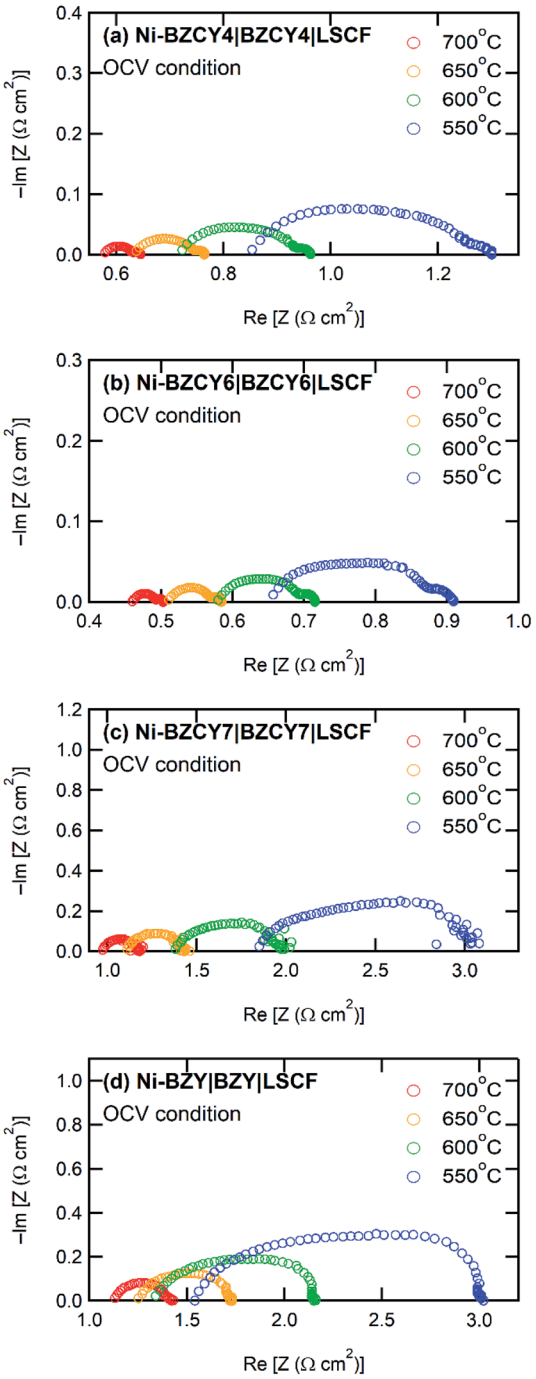

Fig. 6 Electrochemical impedance spectra of anode-supported thin film cells with electrolytes of (a) BZCY4, (b) BZCY6, (c) BZCY7, and (d) BZY in fuel cell atmosphere under OCV condition.

cathodes; the main peaks are assigned to NiO and $BaZr_xCe_{0.8-x}Y_{0.2}O_{3-\delta}$ for all x. The peaks of $BaZr_xCe_{0.8-x}Y_{0.2}O_{3-\delta}$ shift to high 2θ angle with the increasing x, which is due to lattice contraction by the substitution of Ce^{4+} (0.87 Å) with smaller Zr^{4+} (0.72 Å).[17] BZCY4 does not contain any secondary impurity phases, whereas BZCY6, BZCY7, and BZY show a small impurity peak in the vicinity of 32.5°, which is due to the formation of BaY_2NiO_5 (PDF 00-041-0463). It has been reported that such a secondary phase is readily formed by the reaction between BZY and NiO through high-temperature sintering.[18–21] Therefore, the absence of BaY_2NiO_5 impurity phase in BZCY4 is probably due to the low reactivity of $BaCeO_3$ against NiO. EDX analysis confirms that Ba/Zr/Ce/Y molar ratios in all electrolytes are very close to the target ones, indicating that the vaporization of Ba is minimal in our fabrication process.

Fig. 3 shows SEM images of the cross-sections of anode-supported cells after fuel cell tests; all cells comprise three layers: porous LSCF cathodes, dense $BaZr_xCe_{0.8-x}Y_{0.2}O_{3-\delta}$ electrolyte films and porous $Ni/BaZr_xCe_{0.8-x}Y_{0.2}O_{3-\delta}$ cermet anode supports. The recent PCFCs use an electrolyte–electrode composite for the cathode to reduce the cathodic interfacial overpotentials with extended gas–electron–proton triple phase boundaries.[15] In this study, however, a single phase LSCF paste is used as a well-defined cathode in all cells because the objective of this study is to clarify optimal Zr contents of $BaZr_xCe_{0.8-x}Y_{0.2}O_{3-\delta}$ electrolytes to obtain satisfactorily high fuel cell efficiency and excellent CO_2 tolerance simultaneously.

In every case, dense electrolyte films with 30 μm thickness are uniformly formed over a wide area of porous anode supports without apparent cracks or pinholes. The average grain sizes remarkably decrease with the increasing Zr contents. In BZCY4 electrolyte films, the oxide grains exhibit significant growth; their diameter is as large as 5–10 μm (Fig. 3(a)). BZCY6 electrolyte films are also formed by close packing of micrometer grains although the typical grain sizes (4–6 μm) are smaller than those of BZCY4 (Fig. 3(b)). The grain sizes of BZCY7 and BZY are much smaller than those of BZCY6 (Fig. 3(c) and (d)), *i.e.*, they are typically less than 1 μm and thus, their films have a large volume of grain boundaries.[10] In addition, porous precipitates are formed at the grain boundaries in the BZY electrolyte film (Fig. 4), which can be identical to Ni particles formed by the reduction of BaY_2NiO_5 impurity phases under hydrogen atmosphere.[19,22] Such metallic Ni segregation is not observed in BZCY6 and BZCY7, indicating that the reaction between BZCY6 or BZCY7 and NiO is much less pronounced than that with BZY.

3.2 Electrochemical performances

Fig. 5 shows the *I–V* and *I–P* curves of all anode-supported cells along with the summary of open circuit voltages (OCVs) and peak power densities (PPDs). The BZCY4- and BZCY6-based cells exhibit sufficiently high open-circuit voltages (OCVs) of more than 1 V in the measured temperature range, which are close to the theoretical values, suggesting that electronic conduction and gas leakage are sufficiently small in BZCY4 and BZCY6 electrolyte thin films. Hence, the BZCY4- and BZCY6-based cells yield significantly high peak power densities (PPDs). The BZCY4-based cell delivers PPD values of 381, 340, 279, and 205 mW cm^{-2} at 700, 650, 600, and 550 °C, respectively (Fig. 5(f)). Moreover, BZCY6-based cells yield higher PPDs than BZCY4 regardless of the higher Zr contents, and the values reach 435, 396, 336, and 264 mW cm^{-2} in the same temperature range (Fig. 5(f)). However, the fuel cell performances rapidly deteriorate with further Zr substitution. PPD of the BZCY7-based cell is less than 120 mW cm^{-2} even at 600 °C although

Open Access Article. Published on 23 July 2018. Downloaded on 12/15/2025 1:50:24 AM.
This article is licensed under a Creative Commons Attribution-NonCommercial 3.0 Unported Licence.

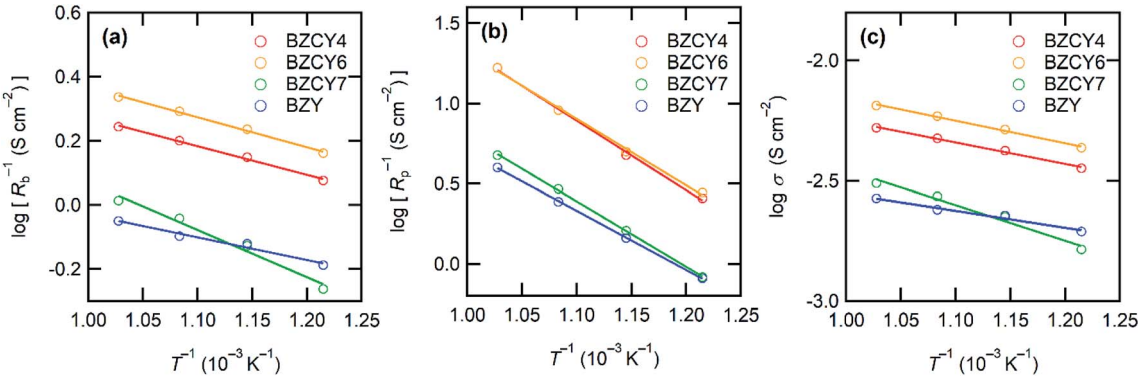

Fig. 7 Arrhenius plots of reciprocal of (a) ohmic resistance (R_b) and (b) polarization resistance (R_p) of anode-supported cells. The values of R_b and R_p are determined from the features of impedance Nyquist plots in Fig. 6. (c) Arrhenius plots of proton conductivities of BZCY4, BZCY6, BZCY7, and BZY electrolyte films determined from R_b and film thickness.

the cell gains OCV of more than 1.0 V at temperatures below 650 °C. PPD of the BZY cell is smaller than that of BZCY7, and OCVs do not reach 1.0 V even at temperatures below 600 °C, which is probably due to electronic leakage mediated *via* metallic Ni precipitates.

To provide further verification for the fuel cell performances, the polarization behavior is studied by electrochemical impedance techniques. Fig. 6 presents the impedance spectra of the fuel cells under OCV conditions. In general, Nyquist plots of the impedance responses of PCFCs provide the *x*-intercept in a high frequency region, corresponding to electrolyte resistances. After the intercept, they exhibit broad semi-arcs mainly due to interfacial polarization resistances at the cathode side;[23] thus, the diameters of the arcs provide polarization resistances. Fig. 7 displays Arrhenius plots of inversed ohmic resistance (R_b) and polarization resistance (R_p) determined from the spectral features of the Nyquist impedance plots. All electrolyte-type cells show Arrhenius-type linear temperature dependence of R_p^{-1} (Fig. 7(b)), and the related activation energies are similar; the values are 0.94, 0.90, 0.89, and 0.81 eV for BZCY4, BZCY6, BZCY7, and BZY-based cells, respectively, which implies that the cathodic reaction involves the same rate-determining steps. R_p values of BZCY4- and BZCY6-based cells are very close each other at all temperatures, whereas R_p values of BZCY7 and BZY

Table 1 Summary of fuel cell performances at 600 °C for recently reported thin film PCFCs with BZCY4, BZCY6, BZY, and $BaZr_{0.1}Ce_{0.7}Y_{0.1}Yb_{0.1}O_{3}$ (BZCYYb) electrolytes fabricated by solid state sintering processes[a]

Anode	Electrolyte	Cathode	R_b/Ω cm^2	Thickness/μm	OCV/V	PPD/ mW cm^{-2}	Film conductivity/ S cm^{-1}	Reference
Ni-BZCY4	BZCY4	LSCF	0.71	30	1.07	279	4.2×10^{-3}	This work
Ni-BZCY6	BZCY6	LSCF	0.58	30	1.08	336	5.2×10^{-3}	This work
Ni-BZCY7	BZCY7	LSCF	1.34	30	1.05	111	2.7×10^{-3}	This work
Ni-BZY	BZY	LSCF	1.32	30	0.93	102	2.2×10^{-3}	This work
Ni-BZCY4	BZCY4	BSCF	—	20	1.04	230	—	5
Ni-BZCY4	BZCY4	BSCF	1.23	35	1.05	159	2.8×10^{-3}	14
Ni-BZCY4	BZCY4	BSCF	0.74	25	1.02	276	3.4×10^{-3}	25
Ni-BZCY4	BZCY4	BSCF	—	35	0.98	151	—	26
Ni-BZY	BZCY4	Pr_2NiO_4	0.77	5	1.03	102	6.5×10^{-4}	28
Ni-BZCY4	BZCY4	BZCY4-BSCFT	0.91	20	1.03	194	2.2×10^{-3}	29
Ni-BZCY6	BZCY6	BSCF	—	25	1.07	116	—	30
Ni-BZY	BZY	BSCF	—	35	1	22	—	14
Ni-BZI	BZI	PBC-BZPY	2.01	15	0.946	84	7.5×10^{-4}	27
Ni-BZY	BZY (PLD)	LSCF-BCYb	1.85	4	0.99	110	2.16×10^{-4}	31
Ni-BZCY	BZY	SSC-SDC	3.24	25	0.97	55	7.7×10^{-4}	32
Ni-BZY	BZYZn	Pt	1.15	20	0.94	75	1.7×10^{-3}	33
Ni-BZY	BZPY	LSCF-BZPY	1.33	20	0.93	81	1.5×10^{-3}	34
Ni-BZY	BZPY	LSCF-BZPY30	0.53	12	0.9	163	2.26×10^{-3}	35
Ni-BZY	BZY (PLD)	LSC	0.15	2	1.0	720	—	36
Ni-BZCYYb (SSRS)	BZCYYb	BCFZY	0.29	30	1.1	660	1.0×10^{-2}	15
Ni-BZCYYb 4411	BZCYYb 4411	PBSCF	0.08	15	1.03	1098	1.88×10^{-2}	37

[a] $La_{0.6}Sr_{0.4}Co_{0.2}Fe_{0.8}O_3$ (LSCF), $Ba_{0.5}Sr_{0.5}Co_{0.8}Fe_{0.2}O_3$ (BSCF), $La_{0.6}Sr_{0.4}CoO_3$ (LSC), $Ba_{0.5}Sr_{0.5}(Co_{0.8}Fe_{0.2})_{0.9}Ti_{0.1}O_3$ (BSCFT), $NdBa_{0.5}Sr_{0.5}Co_{1.5}Fe_{0.5}O_{5+\delta}$ (NBSCF), $BaCo_{0.4}Fe_{0.4}Zr_{0.1}Y_{0.1}O_3$ (BCFZY), $BaZr_{0.85}Y_{0.15}O_3$ (BZY15), $BaCe_{0.9}Yb_{0.1}O_{3-\delta}$ (BCYb), $Sm_{0.5}Sr_{0.5}CoO_{3-\delta}$ (SSC), $Ce_{0.8}Sm_{0.2}O_{2-\delta}$ (SDC), $PrBaCo_2O_{5+\delta}$ (PBC), $BaZr_{0.7}In_{0.3}O_{3-\delta}$ (BZI), $BaZr_{0.1}Ce_{0.7}Y_{0.2}O_{3-\delta}$ (BZCY), $BaZr_{0.8}Y_{0.16}Zn_{0.04}O_{3-\delta}$ (BZYZn), $BaZr_{0.7}Pr_{0.1}Y_{0.2}O_{3-\delta}$ (BZPY), $BaZr_{0.5}Pr_{0.3}Y_{0.2}O_{3-\delta}$ (BZPY30), $BaZr_{0.4}Ce_{0.4}Y_{0.1}Yb_{0.1}O_3$ (BZCYYb4411), $PrBa_{0.5}Sr_{0.5}Co_{1.5}Fe_{0.5}O_{5+\delta}$ (PBSCF).

This journal is © The Royal Society of Chemistry 2018

Open Access Article. Published on 23 July 2018. Downloaded on 12/15/2025 1:50:24 AM.
This article is licensed under a Creative Commons Attribution-NonCommercial 3.0 Unported Licence.

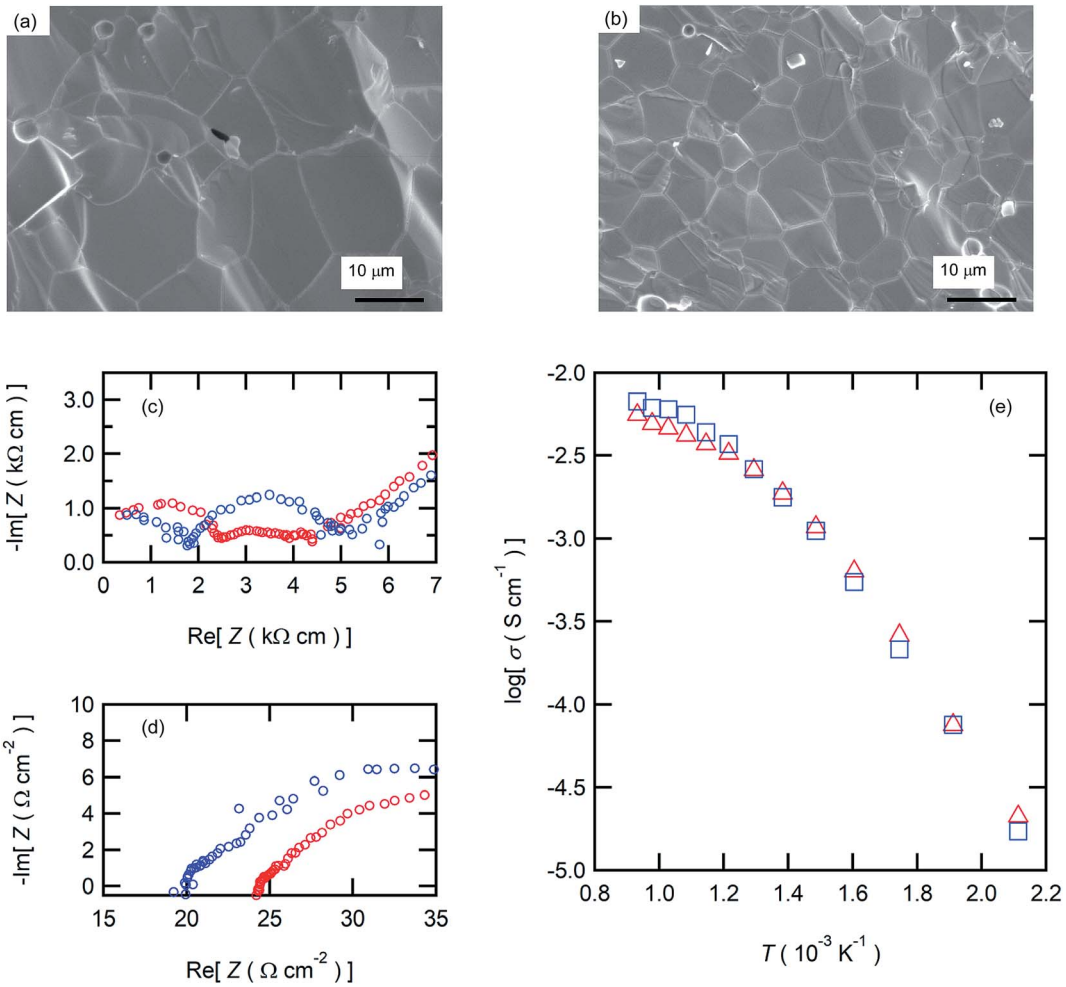

Fig. 8 Cross-sectional SEM micrographs of thermally etched (a) BZCY4 and (b) BZCY6 sintered discs. Impedance responses of the sintered discs measured in wet 10%-H_2/Ar at (c) 200 °C and (d) 600 °C (○: BZCY4 and ○: BZCY6); (e) Arrhenius plots of total conductivity of the sintered discs (△: BZCY4 and □: BZCY6).

are one order of magnitude larger than the former values, which is probably due to their low proton conductivity,[10] as mentioned below.

R_b^{-1} obeys linear Arrhenius-type relationship, providing the activation energies of proton conduction of 0.26, 0.33, 0.34, and 0.22 eV for BZCY4, BZCY6, BZCY7, and BZY cells, respectively, and these energies are similar to the corresponding energies reported elsewhere.[24–27,31] In all electrolyte cells, the fractions of R_b to total resistances (R_b + R_p) account for 65–80% at 600 °C, indicating that the electrolyte resistances involve the major part of the voltage losses. R_b values of BZCY7 and BZY electrolyte films are one order of magnitude higher than those of BZCY4 and BZCY6, which is due to large grain boundary resistances; the grain boundary volumes of the former are much larger than those of the latter (Fig. 3). The BZCY6-based cell has the lowest ohmic resistance among the four cells (Fig. 6), which is the main reason for obtaining the highest PPD value with the BZCY6-based cell.

The performances of recently reported PCFCs with BZCY4, BZCY6, BZCY7 and BZY electrolyte thin films at 600 °C are summarized in Table 1 for direct comparison; most of these materials were fabricated using chemically synthesized fine powders of $BaZr_xCe_{0.8-x}Y_{0.2}O_3$ for sintering.[5,14,25–36] In recent years, S. Choi *et al.* reported outstanding performances of $BaZr_{0.4}Ce_{0.4}Y_{0.1}Yb_{0.1}O_{3-\delta}$-based cells with a $PrBa_{0.5}Sr_{0.5}Co_{1.5}Fe_{0.5}O_{5+\delta}$ cathodic interlayer, which reached to about 1.1 W cm^{-2} at 600 °C.[37] Although PPD of our BZCY4 cells is lower than this significant result, it is higher than the PPD values reported elsewhere for the anode-supported PCFCs with the same electrolyte[5,14,25,26,29] (Table 1). Moreover, the studies on BZCY6 cells are rather rare,[30] and PPD of our BZCY6 cells is 3 times higher than that of the analogous cell fabricated with sol–gel-derived fine powders (116 mW cm^{-2}).[30] This behavior could be related to the sufficiently low grain boundary resistances of our electrolyte films because the average grain size of our BZCY6 was larger than those of the previously reported cells (ref. 16). Although the BZCY7- and BZY-based cells prepared here possessed low fuel cell performances compared to the other two, their PPDs were higher than those of most of the analogous-electrolyte fuel cells[14,27–34] (Table 1). Moreover, PPD of

Open Access Article. Published on 23 July 2018. Downloaded on 12/15/2025 1:50:24 AM.
This article is licensed under a Creative Commons Attribution-NonCommercial 3.0 Unported Licence.

our BZY cell is comparable to that reported for BZY-based thin film fuel cells fabricated by pulsed laser deposition (PLD) at 600 °C (ref. 31) (Table 1). It can be concluded that all electrolyte cells prepared here have equivalent or higher efficiencies than the corresponding high-performance fuel cells reported elsewhere. These features prove that the upper limit of Zr contents in $BaZr_xCe_{0.8-x}Y_{0.2}O_{3-\delta}$ electrolytes is near $x = 0.6$ to develop a low-resistive, large-grained electrolyte film *via* a low-temperature reactive sintering process.

The aforementioned results clearly demonstrate that the BZCY6 cells exhibit superior fuel cell performances compared to BZCY4 cells in spite of the higher Zr contents and smaller grain sizes. Fig. 7(c) displays the proton conductivity (σ) of the electrolyte films determined from R_b and film thickness; BZCY6 has higher conductivity than BZCY4 even though the grain boundary volumes of the former are apparently larger than those of the later. To verify this point, we examine the proton conductivities of BZCY4 and BZCY6 bulk ceramics prepared by an SSRS process that is similar to the one used for the fabrication of anode-supported cells. The BZCY4 and BZCY6 ceramics thus prepared have highly dense matrices (relative density of >97%), with grain sizes equal to 10 and 5 μm diameter, respectively (Fig. 8(a) and (b)); these results are in agreement with the grain sizes observed for the thin film fuel cell (Fig. 3). The impedance spectra of both ceramics show apparent bulk and interfacial contributions in high (10^6–10^5 Hz) and middle (10^5–10^2 Hz) frequency ranges, respectively, at relatively low temperatures together with electrode contribution in low frequency region (<10^2 Hz), as shown in Fig. 8(c). The bulk resistance of BZCY6 is lower than that of BZCY4, whereas the interfacial resistance of BZCY6 is higher than that of BZCY4 and thus, the total resistance of BZCY6 is 20% larger than that of BZCY4 at 200 °C; after increasing the temperature to 550 °C, both show only an x-intercept in the frequency range of 10^6–10^4 Hz due to sufficiently reduced resistances.[9] The x-intercept of BZCY6 is clearly smaller than that of BZCY4 at 550 °C.

Fig. 8(e) displays the Arrhenius plots of the total conductivity of the BZCY4 and BZCY6 bulk ceramics determined by the sum of the bulk resistances and grain-boundary resistances. In both, the slopes of the plots change at around 400 °C, indicating that dominant conduction mechanism has changed at this temperature. For many $BaZr_xCe_{0.8-x}Y_{0.2}O_{3-\delta}$ systems, it has been reported that the grain boundary resistances are dominant in the low-temperature region, whereas these are smaller than the bulk resistances in the high-temperature region, because the activation energies of grain boundary conduction are larger than those of the bulk.[38] Accordingly, the relatively high total conductivity of BZCY6 can be due to the bulk conductivity being higher than that of BZCY4 (Fig. 8(e)). In fact, this feature is in agreement with the previously reported result.[9] These results prove that the superior fuel cell performances of BZCY6 can be due to relatively high proton conductivities in the IT ranges.

Finally, we examined the durability of BZCY6 under CO_2-containing fuel conditions. Fig. 9(a) shows current decays of BZCY6 cells in potentiostatic operation at 0.7 V with 1% CO_2-containing hydrogen fuels. The cell keeps outputting a constant current of about 330 mA cm^{-2} for 2 days with CO_2-containing fuels although the current slightly decreases just after the introduction of CO_2. XRD measurements of the BZCY6 cell after durability tests confirm that decomposition products such as $BaCO_3$, ZrO_2 and CeO_2 are not formed even after fuel cell operations for several hours under a CO_2 atmosphere (Fig. 9(b)), which reveals that BZCY6 is thermodynamically stable under CO_2-containing fuel conditions. The current results unambiguously demonstrate that BZCY6 is a promising electrolyte for intermediate temperature PCFC with excellent low-temperature sinterability and CO_2 tolerance.

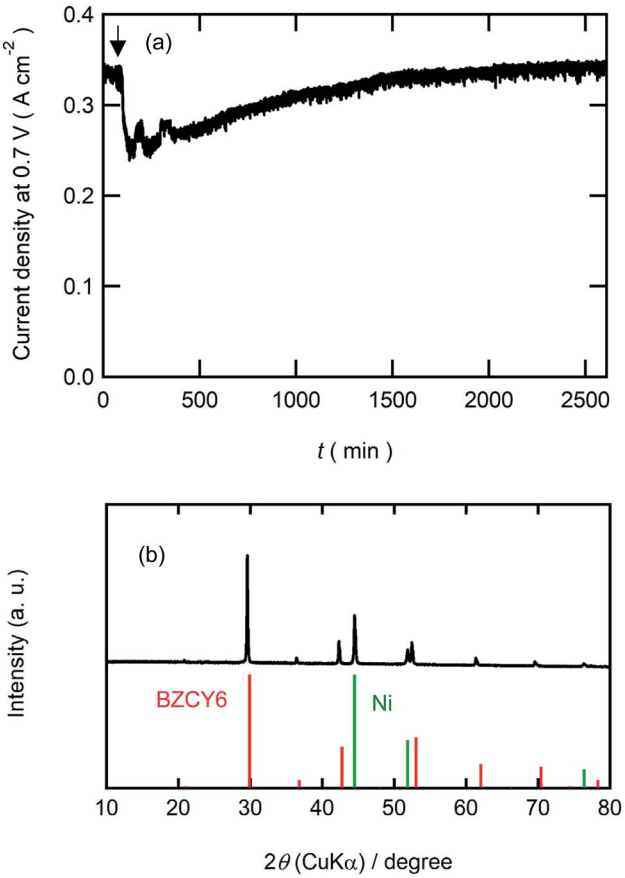

Fig. 9 Durability test of BZCY6 cell. (a) Current decays of BZCY6 cells in a potentiostatic run at 0.7 V using 1% CO_2-containing hydrogen fuels. The arrow indicates the time to start CO_2 flow. (b) XRD pattern of BZCY6 cells after fuel cell under CO_2-containing fuel conditions. Red and green lines indicate the theoretical patterns of $BaCe_{0.9}Y_{0.1}O_3$ (JCPDS 82-2372) and Ni (JCPDS 04-850).

4. Conclusion

Herein, high performance anode-supported cells with Zr-rich $BaZr_xCe_{0.8-x}Y_{0.2}O_3$ ($x = 0.4$, 0.6, 0.7, and 0.8) were successfully fabricated by solid-state reactive sintering (SSRS) with $Zn(NO_3)_2$ additives by a single sintering step at 1400 °C. For $x = 0.4$ and 0.6, $BaZr_xCe_{0.8-x}Y_{0.2}O_3$ ceramics exhibited excellent sinterability and thus, densely packed films comprising μm-sized grains were obtained by sintering at a relatively low temperature with the aid of Zn additives. According to the large-grained

This journal is © The Royal Society of Chemistry 2018

Open Access Article. Published on 23 July 2018. Downloaded on 12/15/2025 1:50:24 AM.
This article is licensed under a Creative Commons Attribution-NonCommercial 3.0 Unported Licence.

microstructures, the ohmic resistances of these electrolyte films were smaller than those reported for the analogous thin film and thus, the cells with $x = 0.4$ and 0.6 exhibited highly efficient power generation, yielding peak power densities of 279 and 336 mW cm^{-2} at 600 °C, respectively, which were comparable to or several times higher than those of the analogous thin film fuel cells prepared from sol–gel-derived $BaZr_xCe_{0.8-x}Y_{0.2}O_3$ powders. $BaZr_{0.6}Ce_{0.2}Y_{0.2}O_3$ was found to have higher proton conductivity than $BaZr_{0.4}Ce_{0.4}Y_{0.2}O_3$ at temperatures above 500 °C despite the relatively high Zr contents and thus, it showed excellent durability under CO_2-containing atmosphere. The preceding results encourage the development of high-performance PCFCs with thermally stable, Zr-enriched $BaZr_{0.6}Ce_{0.2}Y_{0.2}O_3$ electrolytes.

Conflicts of interest

There are no conflicts to declare.

Acknowledgements

This work was granted by MIRAI project (JPMJMI17E8) of Japanese Agency of Science and Technology (JST). A part of this work was conducted at Laboratory of XPS analysis, Joint-use facilities, Hokkaido University, supported by "Material Analysis and Structure Analysis Open Unit (MASAOU)".

References

1 E. P. Murray, T. Tsai and S. A. Barnett, *Nature*, 1999, **400**, 649.
2 E. Ivers-Tiffée, *et al.*, *J. Eur. Ceram. Soc.*, 2001, **21**, 1805.
3 A. Boudghene Stambouli and E. Traversa, *Renewable Sustainable Energy Rev.*, 2002, **6**, 433.
4 A. Esquirol, N. P. Brandon, J. A. Kilner and M. Mogensen, *J. Electrochem. Soc.*, 2004, **151**, A1847.
5 Y. Guo, R. Ran and Z. Shao, *Int. J. Hydrogen Energy*, 2010, **35**, 5611.
6 K. D. Kreuer, *Annu. Rev. Mater. Res.*, 2003, **33**, 333.
7 W. Zajac, D. Rusinek, K. Zheng and J. Molenda, *Cent. Eur. J. Chem.*, 2013, **11**, 471.
8 K. Katahira, Y. Kohchi, T. Shimura and H. Iwahara, *Solid State Ionics*, 2000, **138**, 91.
9 P. Sawant, S. Varma, B. N. Wani and S. R. Bharadwaj, *Int. J. Hydrogen Energy*, 2012, **37**, 3848.
10 E. Fabbri, A. D'Epifanio, E. D. Bartolomeo, S. Licoccia and E. Traversa, *Solid State Ionics*, 2008, **179**, 558.
11 S. B. C. Duval, P. Holtappels, U. F. Vogt, U. Stimming and T. Graule, *Fuel Cells*, 2009, **9**, 613.
12 S. M. Haile, G. Staneff and K. H. Ryu, *J. Mater. Sci.*, 2001, **36**, 1149.
13 E. Fabbri, D. Pergolesi and E. Traversa, *Chem. Soc. Rev.*, 2010, **39**, 4355.
14 Y. Guo, Y. Liu, R. Ran and Z. Shao, *J. Power Sources*, 2009, **193**, 400.
15 C. Duan, J. Tong, M. Shang, S. Nikodemski, M. Sanders, S. Ricote, A. Almansoori and R. O'Hayre, *Science*, 2015, **349**, 1321.
16 S. Nikodemski, J. Tong and R. O'Hayre, *Solid State Ionics*, 2013, **253**, 201.
17 R. D. Shannon, *Acta Crystallogr., Sect. A: Cryst. Phys., Diffr., Theor. Gen. Crystallogr.*, 1976, **32**, 751.
18 J. Tong, D. Clark, M. Hoban and R. O'Hayre, *Solid State Ionics*, 2010, **181**, 496.
19 J. Tong, D. Clark, L. Bernau, A. Subramaniyan and R. O'Hayre, *Solid State Ionics*, 2010, **181**, 1486.
20 L. Bi, E. Fabbri, Z. Sun and E. Traversa, *Energy Environ. Sci.*, 2011, **4**, 1352.
21 J. Tong, D. Clark, L. Bernau, M. Sanders and R. O'Hayre, *J. Mater. Chem.*, 2010, **20**, 6333.
22 W. G. Coors, *"Protonic ceramics of the solid solution BaCexZr0.8−xY0.2O3−δ prepared by NiO-reactive sintering. Part I: fabrication and microstructure", CoorsTek report* (available from the author), March 18th, 2010.
23 A. Jun, J. Kim, J. Shin and G. Kim, *ChemElectroChem*, 2016, **3**, 511.
24 S. H. Nien, C. S. Hsu, C. L. Chang and B. H. Hwang, *Fuel Cells*, 2011, **11**, 178.
25 Y. Liu, Y. Guo, R. Ran and Z. Shao, *J. Membr. Sci.*, 2013, **437**, 189.
26 Y. Guo, R. Ran and Z. Shao, *Int. J. Hydrogen Energy*, 2011, **36**, 1683.
27 L. Bi, E. Fabbri, Z. Sun and E. Traversa, *Solid State Ionics*, 2011, **196**, 59.
28 N. Nasani, D. Ramasamy, S. Mikhalev, A. V. Kovalevsky and D. P. Fagg, *J. Power Sources*, 2015, **278**, 582.
29 L. Bi, E. Fabbri and E. Traversa, *Electrochem. Commun.*, 2012, **16**, 37.
30 Y. Liu, R. Ran, M. O. Tade and Z. Shao, *J. Membr. Sci.*, 2014, **467**, 100.
31 D. Pergolesi, E. Fabbri and E. Traversa, *Electrochem. Commun.*, 2010, **12**, 977.
32 J. Xiao, W. P. Sun, Z. W. Zhu, Z. T. Tao and W. Liu, *Mater. Lett.*, 2012, **73**, 198.
33 I. Liusetto, S. Licoccia, A. D'Epifanio, A. Sanson, E. Mercadelli and E. Di Bartolomeo, *J. Power Sources*, 2012, **220**, 280.
34 E. Fabbri, L. Bi, H. Tanaka, D. Pergolesi and E. Traversa, *Adv. Funct. Mater.*, 2011, **21**, 158.
35 E. Fabbri, L. Bi, J. L. M. Rupp, D. Pergolesi and E. Traversa, *RSC Adv.*, 2011, **1**, 1183.
36 K. Bae, D. Y. Jang, H. J. Choi, D. Kim, J. Hong, B. K. Kim, J. H. Lee, J. W. Son and J. H. Shim, *Nat. Commun.*, 2017, **8**, 14553.
37 S. Choi, C. J. Kucharczyk, Y. Liang, X. Zhang, I. Takeuchi, H. Ji and S. M. Haile, *Nat. Energy*, 2018, **3**, 202.
38 S. Ricote, N. Bonanos, A. Manerbino and W. G. Coors, *Int. J. Hydrogen Energy*, 2012, **37**, 7954.